LASER INTERFEROMETER GRAVITATIONAL WAVE OBSERVATORY

- LIGO -

CALIFORNIA INSTITUTE OF TECHNOLOGY
MASSACHUSETTS INSTITUTE OF TECHNOLOGY

technical note	**LIGO-T950029-01 -R**		5/8/95
Document Type	*Doc Number*	*Group-Id*	*Date*

Installation of Monolithic Test Masses in the 40 m Interferometer

Title

Aaron Gillespie

Author(s)

This is an internal working note of the LIGO Project

California Institute of Technology
LIGO Project - MS 102-33
Pasadena CA 91125
Phone (818) 395-2966
Fax (818) 304-9834
E-mail: info@ligo.caltech.edu
WWW: http://www.ligo.caltech.edu

1 ABSTRACT

This paper is a complete summary of recently completed work to install new test masses in the 40-meter inteferometer at Caltech. It is intended to be used primarily within the LIGO project for documentation. Discussed here are the motivations for the work including some history and the thermal noise predictions of the old test masses, a detailed description of the experimental work done in the suspension development apparatus which lead to the present design of the magnet attachments, and the results of the installation of the new test masses. A less detailed report which concentrates only on the results of the installation in the 40-meter interferometer is available in LIGO technical report TR94-7.

2 MOTIVATION

2.1 Background

In late 1991 and early 1992 two improvements were made in the interferometer's performance which increased the priority of the installation of the new test masses. First, new orientation control systems were installed which greatly reduced the noise below 1 kHz,[1] and second, the laser power at the input of the interferometer was increased, reducing the shot noise and thus improving the interferometer performance at higher frequencies. These two improvements left a region in the noise spectrum between 500 Hz and 1.5 kHz where the noise was a slowly varying function of frequency and of unknown origin (see Figure 1 on page 4).

In attempting to explain this region of the noise spectrum, many potential noise sources were ruled out. Any sort of mechanical excitation above thermal noise transmitted through the suspension wires could be ruled out since the violin resonances were at thermally excited levels.[2] Frequency noise and amplitude noise on the light and electronics noise in the readout and coil driver were measured and eliminated as potential noise sources. Noise due to scattered light was a possibility because there was much scattered light in the restricted vacuum system of the 40-meter at that time, but there were no models describing how the scattered light would couple to the interferometer noise at the observed level. In 1993, the Mark II version of the interferometer with its expanded vacuum system became operational. That change made a qualitatively radical change in the scattered light, but the unexplained region of the interferometer noise spectrum remained unchanged, eliminating scattered light as a likely noise source. In addition, the improvements in the seismic isolation of the Mark II reduced the seismic noise, extending the unexplained and slowly varying region of the noise spectrum down to 200 Hz (Figure 1 on page 4).

2.2 Internal thermal noise

One remaining possibility for this noise was thermal noise in the internal vibrations of the test mass. The mechanical quality factors of the old test masses were measured and found to be lower than expected from measurements done before the test masses were installed. The existing test

1. S. Kawamura and M. Zucker, Mirror-orientation noise in a Fabry-Perot interferometer gravitational-wave detector, *Appl Opt.*, 33 3912 (1994).
2. A. Gillespie and F. Raab, Thermal noise in the test mass suspensions of a laser interferometer gravitational-wave detector prototype, *Phys Lett A*, 178 357 (1993).

masses were fused silica cylinders 10 cm in diameter and 8.8 cm long. A 25 mm hole was bored through the center and a 38 mm mirror was optically contacted on one face. The faces of the test masses were polished; the sides were not. A summary of the measurements of the Q's of the axisymmetric modes of these test masses are in Table 1 on page 2. The Q measurements were made by sweeping a driving force through the resonance and measuring the FWHM of the frequency response of the interferometer output. For the end masses the driving force was applied by the driving coils near magnets attached to the masses; for the vertex masses the driving force was elctrostatic. These modes were identified as the axisymmetric modes by the following procedure. The approximate resonant frequencies of the axisymmetric modes were found using finite element analysis. The most strongly excited modes near the appropriate frequency were identified as the axisymmetric modes. (Non-axisymmetric modes have nodes at the mirror center where the light sampled the motion and hence are weakly coupled to the interferometer.)

Table 1: Q's of old test masses as installed in 40-meter interferometer.

mirror	*resonant frequency (Hz)*	*Q*
East End	27416 27673 34748	2700 5100 33100
East Vertex	27240 27580	800 2000
South Vertex	27395 27576	30000 1700
South End	27436 27996 34748	54900 14400 41100

The spectral density of the displacement, $S_x(f)$, due to the thermal noise of the internal vibrational modes can be calculated by summing the general thermal noise lineshape over all modes:[3]

$$S_x(f) = \sum_n \frac{4k_B T \varphi_n(\omega)}{\alpha_n m \omega_n^2 \omega}$$

k_B, T, m, and α_n are Boltzman's constant, the temperature, the mass, and the effective mass coefficient of the n^{th} mode; and ω, ω_n, and $\varphi_n(\omega)$ are the angular frequency (corresponding to $2\pi f$), the angular resonant frequency of the n^{th} mode, and the loss function of the n^{th} mode. In order to estimate the off resonance thermal noise from these Q's, several assumptions must be

3. A. Gillespie and F. Raab, Thermally excited vibrations of the mirrors of laser interferometer gravitational-wave detectors, to be published in *Phys Rev D*, (1995).

made. First, the loss function was assumed to be independent of frequency. This assumption enabled the loss function to be defined as

$$\varphi_n(\omega) = \frac{1}{Q_n}$$

This assumption was driven primarily by a desire to get a thermal noise prediction that was close to the measured noise spectrum. Any weak frequency dependence could give the appropriate noise level. Second, the effective mass coefficients must be determined. Since these masses were not solid right circular cylinders, calculation of the coefficients was difficult. We simply assumed effective mass coefficients of 0.5 for all modes. Lastly, one must decide how many modes to consider. In principle, all modes with acoustic wavelengths larger than the laser spot size could contribute to the low frequency thermal noise. In this case, all the modes had different Q's, and determining the Q's of the higher order modes was not possible. We assumed that the noise was dominated by the few lower frequency low Q modes that were measured and did not include the higher order modes.

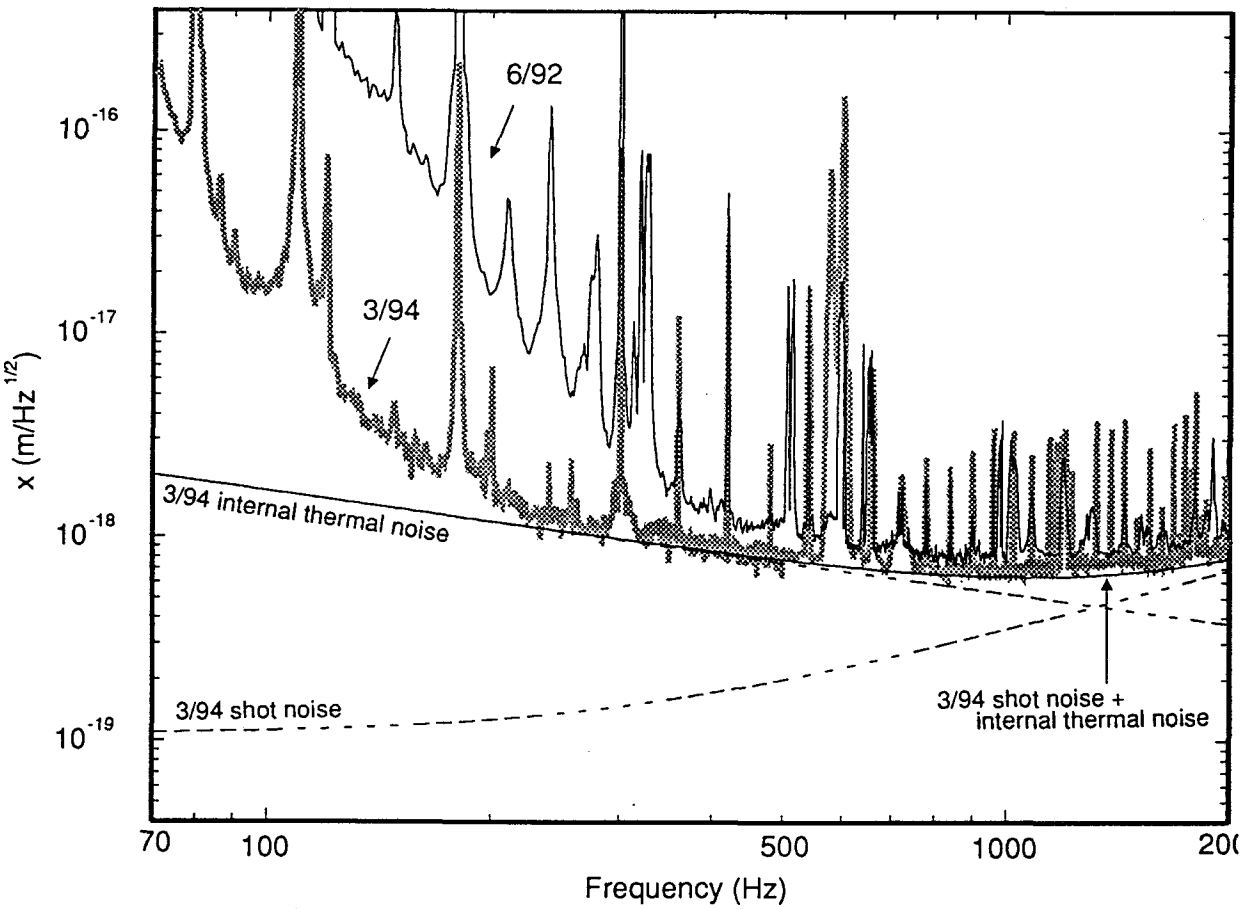

Figure 1: 40-meter interferometer noise spectrum in March 1994. Also shown are the internal vibrational thermal noise estimate and the shot noise.

Given these assumptions, the predicted noise level at 500 Hz was 8×10^{-19} m/$\sqrt{Hz}$, consistent with the observed noise level. The prediction of the internal thermal noise, the predicted shot noise, and the noise spectrum are shown in Figure 1 on page 4. The absolute level of the noise

was adjusted (by 10%), keeping the shape fixed, to give maximum agreement between the noise prediction of internal thermal noise plus shot noise to the observed noise spectrum. Such an adjustment was justified given the uncertainties of the prediction; in fact we were prepared to allow an adjustment of up to a factor of 3. The thermal noise plus shot noise model gave excellent agreement with the noise spectrum above 250 Hz. With this prediction, reduction of internal thermal noise was made a priority after the shakedown of the Mark II interferometer.

3 EXPERIMENTS TO IMPROVE THE Q

3.1 Starting point

An experimental program to improve the Q's of the test mass was begun in early 1992. The old test masses would be replaced with new test masses that had been ordered. The new test mass were 10 cm diameter and 8.8 cm long solid fused silica cylinders. They were polished on all surfaces and had the mirror surface coated directly on one face. The new mirrors had the apparent advantages of their monolithic design (no optical contacts) and their polish on all surfaces. These properties were fixed and their effects were not investigated; they are believed to be improvements. The new mirrors were also higher optical quality.

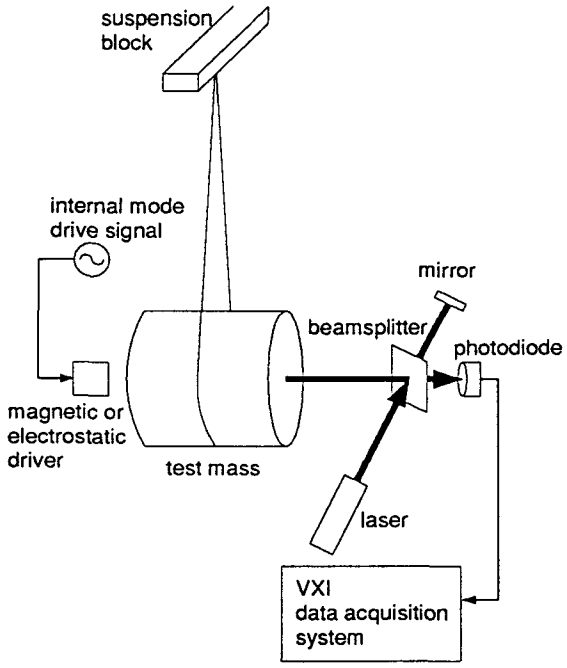

Figure 2: Schematic view of the suspension development apparatus.

The suspension development apparatus, shown schematically in Figure 2 on page 5 was used to evaluate the Q's of various test mass suspension configurations. The Q's were determined by exciting a particular resonance, turning off the excitation, and measuring the decay time of the oscillation. For configurations with magnets, a magnetic driver was used to excite the resonance; for configurations with no magnets, an electrostatic driver[4] was used. For each suspension config-

4. A. Cadez and A. Abramovici, Measuring high mechanical quality factors of bodies made of bare insulating materials, *J Phys E: Sci Instrum*, **21** 453 (1988).

uration, the Q's of the five lowest frequency axisymmetric modes, shown in Figure 3 on page 6, were evaluated.

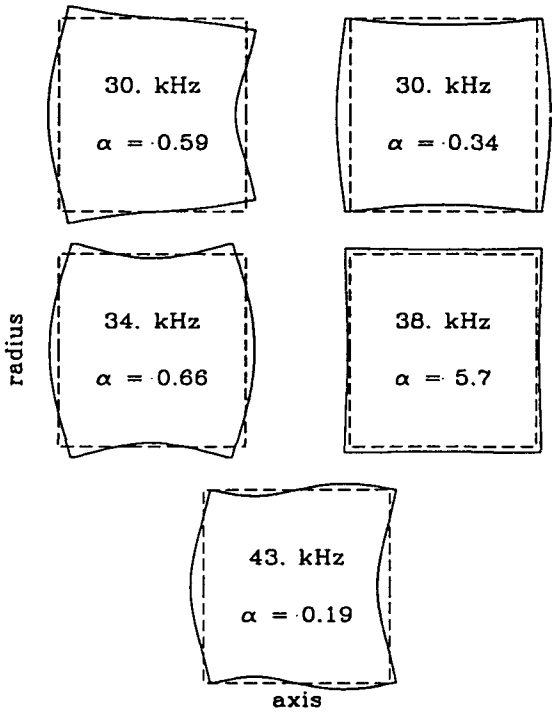

Figure 3: Five lowest frequency axisymmetric modes.

3.2 Initial Measurements

The simplest suspension configuration, and the one in which the least additional loss above the intrinsic loss in the fused silica might be expected, is to suspend the test mass in a single wire loop with no magnets attached. The results of such a set of measurements are given in Table 2 on page 7. The Q's of all modes except the 30.2 kHz mode were above 5×10^6. The 30.2 kHz mode was excessively damped by the suspension wire. That mode is the only one with substantial axial motion at the center where the wire is situated (see the left 30 kHz mode in Figure 3 on page 6). With no well defined attachment point, the wire was free to rub against the side of the test mass as the test mass vibrated in that mode.

In the next two configurations the suspension wires were moved to the positions which they would occupy in the interferometer. Two wire loops were placed 25 mm apart. In one case the test mass simply sat in the wire loops, in another the points at which the wires leave the mass were defined by epoxying small (1 mm diameter by 3 mm long) fused silica rods on the test mass. Results from these two configurations are shown in the second and third columns of Table 2 on page 7. Notice that the Q's in four modes are slightly degraded from the single wire loop configuration, but with the wires position better defined, the 30.2 kHz mode's Q actually improved. The configuration with the fused silica rods was adopted for the vertex masses in the 40-meter interferometer (see Table 5 on page 16).

The test masses used at the ends of the 40-meter interferometer required magnets be attached to

them for control purposes. Column 4 of Table 2 on page 7 shows the Q's when two 6 mm diameter by 6 mm long neodymium-iron-boron magnets were glued near the edges of the mass. The Q's were degraded by three orders of magnitude for some modes and varied by several orders of magnitude among the modes. To test whether this degradation was a property of the magnetic field, the magnets were baked at 200 C for two weeks to reduce their dipole moments to 0.5% of their original values. The data for the demagnetized magnets is shown in column 5 of Table 2 on page 7. The magnetic field strength had no effect on the Q's. In addition, to test for the possibility that the glue was responsible for the additional loss, two different types of glue were used: a cyano-acrylate glue and a vacuum sealant epoxy. There was no difference in the Q's depending on the type of glue. These results indicated that the dominant loss mechanism was due to the magnets themselves and not due to the magnetic field or the glue joints.

Table 2: Test mass Q's: effects of attachments.

mode resonant frequency (kHz)	*simple single loop* $Q\ (10^3)$	*2 wire loops* $Q\ (10^3)$	*with fused silica rods* $Q\ (10^3)$	*with magnets* $Q\ (10^3)$	*demagnetized magnets* $Q\ (10^3)$
30.2	230	3,200	3,600	9.8	8.6
30.7	9,100	7,100	1,800	890	830
34.7	5,700	4,500	3,100	3.3	3.0
39.0	6,900		940		20.
44.0	5,500	8,100	7,300		180.

3.3 Reducing the losses due to the magnets

The magnitude of the losses in the new masses due to the magnets were of the same order as the losses of the old existing masses in the 40-m interferometer (Table 1 on page 3). Therefore in order to make a substantial improvement in the interferometer noise performance, the exact nature of the loss mechanism was investigated. There are three simple ways in which mechanical energy can be coupled into the magnets from the test mass. One is through motion perpendicular to the attachment joint, or axial motion; another is through motion parallel to the connection joint, or radial motion; and the last is through expansion across the connection joint, or strain motion. The amounts of each of these motions at the point of the magnet attachment were computed for each mode, and quantities that were inversely proportional to the energy were constructed. These constructed quantities--(1/axial motion^2), (1/radial motion^2), and (1/strain^2)--would be proportional to the Q if that particular type of energy transfer dominated the losses. The measured Q's were plotted against these constructed quantities to look for proportionalities.

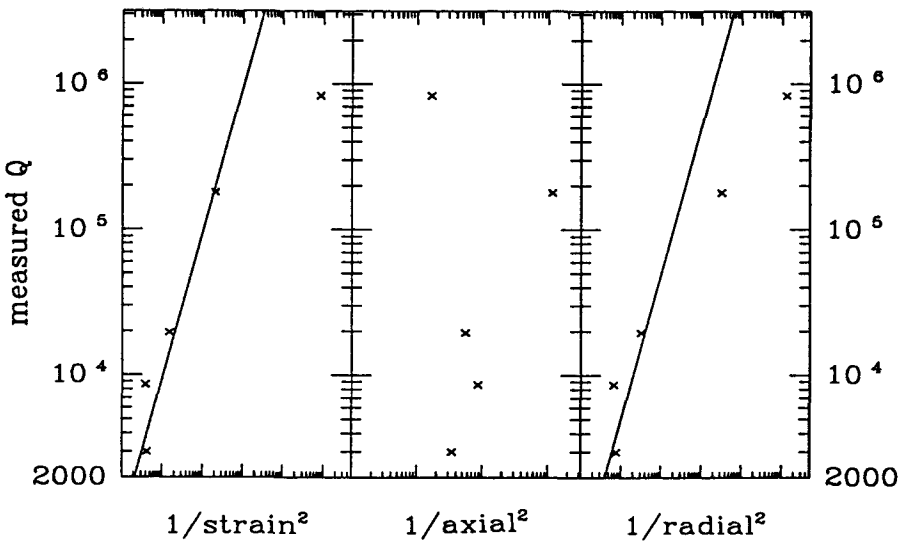

Figure 4: Comparison of measured Q with 3 possible loss mechanisms: couplings of strain energy, axial motion energy, and radial motion energy into the magnets.

Such a plot is shown in Figure 4 on page 8. The demagnetized magnet data were used since those data were most complete.[5] At the factor of three level, four points of the strain damping model and three points of the radial motion damping model lie on a line of direct proportionality. The axial damping motion can be ruled out. For both the strain damping model and the radial damping model, the points that do not fit on the line are the higher Q modes, which have additional damping. There could be some additional damping mechanism that dominates the weakly damped modes but not the strongly damped modes. If the points had fallen on the other side of the proportionality line, or were insufficiently damped in a particular model, then that model could have been ruled out.

Distinguishing between the strain and radial damping models requires additional information which is not on the plot. For the four lowest frequency modes, the face of the test mass undergoes uniform expansion, so that the strain at a particular point is proportional to the radial motion (see Figure 3 on page 6). Only the 43 kHz mode does not have uniform expansion across the face of the mass. This fact is why the radial and strain damping model plots look similar except for at one point. That point is the mode with the Q of 180,000. For the strain damping model the point lies on the direct proportionality line and for the radial damping model it does not. For this reason, the strain damping model was the strongest candidate for the cause of the damping.

Strain energy is coupled between two elements through a surface area. Therefore, the most logical step to minimize the damping would be to minimize the area of contact between the magnet and the test mass. The first step was to verify that this worked, so smaller (3 mm diameter by 5 mm long) magnets were attached to the mass and the Q's were measured. These results are shown in

5. Chronologically, the measurement with the magnets attached was the earliest measurement made. At that time the interferometer was not sensitive enough to measure the Q's of the two higher frequency modes. Since the demagnetized magnet Q's were equivalent to the magnetized magnet Q's for three modes, they were assumed to be equivalent for all modes, and the magnetized magnet measurement was never repeated with the more sensitive interferometer.

column 2 of Table 3 on page 9. The Q's were increased by factors of approximately four for all modes. This improvement was consistent with the hypothesis that the dominant loss mechanism was the coupling of strain into the magnets, but was not sufficient to meet the goal of reducing convincingly the noise in the 40-m interferometer. It was also apparent that magnets which were small enough to meet the goal probably could not be used.

To further reduce the damping, the magnets were not attached directly to the test mass, but rather thin spacers were inserted between the magnets and the masses to attenuate the strain reaching the magnets. Aluminum (for speed and ease of construction) spacers 1.5 mm in diameter and 3 mm long were designed. The Q's were measured with the spacers (and no magnets) attached to the test mass (column 3 of Table 3 on page 9). The results were very promising, so the large magnets were attached to the ends of the spacers. Those Q's are given in column 4 of Table 3 on page 9. The low Q's obtained with the spacers and magnets were initially disappointing and could not be explained with the simple axial, radial, and strain damping models. A full explanation required the consideration of the resonances of the spacer.

Table 3: Test mass Q's: effects of the magnets and spacers.

resonant frequency (kHz)	*with large magnets Q (10^3)*	*with small magnets Q (10^3)*	*with Al spacers only Q (10^3)*	*spacers and big magnets Q (10^3)*	*effective low frequency Q (10^3)*
30.2	8.6	44.	1,600	86	190
30.7	830	4,000	3,600	250	4,500
34.7	3.0	9.1	970	53	200
39.0	20.		2,600	350	940
44.0	180	380	1,300	400	1,500

The observed losses could be explained by damping due to a combination of strain transmitted through the aluminum spacer to the magnet and axial motion coupled into the longitudinal spring mode of the aluminum spacer. The energy coupled into the longitudinal spring mode as a function of frequency is

$$E(\omega) \propto \frac{\omega^4}{\left(\omega_0^2 - \omega^2\right)^2 + \omega^4 \varphi_{spacer}^2(\omega)} x_{axial}^2$$

(the damping is proportional to the energy coupled into the spacer). A plot of such a function is given in Figure 5 on page 10. Well below the resonant frequency, the spacer acts as a rigid body. It is not compressed and no energy is coupled into it. Well above the resonant frequency the spacer is compressed and stretched by the amount of the axial motion and the energy coupling becomes independent of frequency. Near the resonant frequency, the spacer resonance is excited and the damping is enhanced.

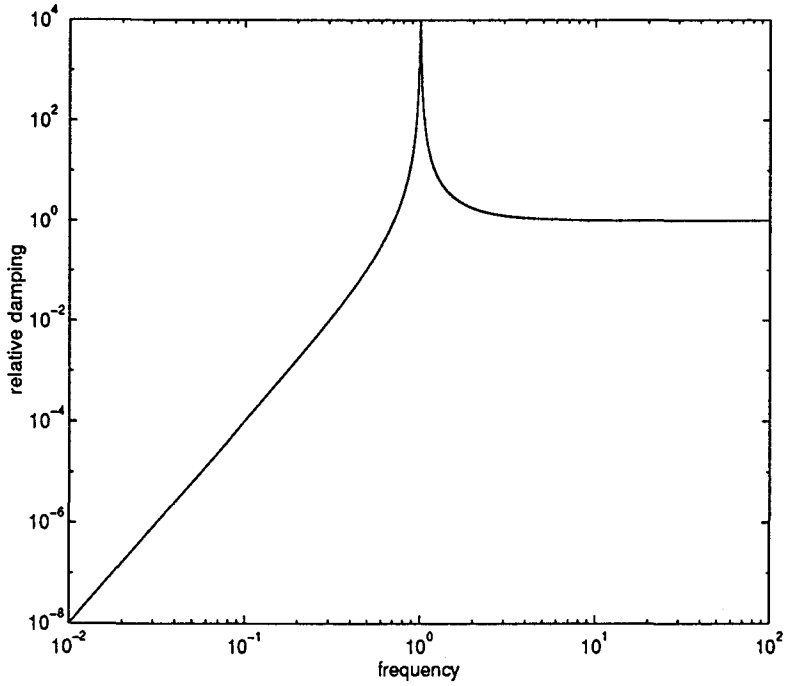

Figure 5: Damping function of test mass due longitudinal spacer mode. On this plot $\omega_0 = 1.$ **and** $\varphi_{spacer}(\omega) = 0.01.$

The measured losses are compared to the model of strain damping plus longitudinal spring mode damping in Figure 6 on page 11. The spacer resonant frequency was about 25 kHz. The ten points came from two sets of measurements on the five modes. One set of measurements was done with the magnets and spacers attached 13 mm from the edge of the mass and the other was done with the magnets at the edge of the test mass. These two sets gave two different sets of samplings of the strain and axial motion of the test mass and gave the additional number of points necessary to do a multi-parameter fit to the damping model. All of the points agree with the model except a few high Q points which show excess damping.

Since the frequencies of interest for the 40-m interferometer and LIGO (100 Hz-1kHz) are well below the spacer resonant frequency and since the spacer damping falls off quickly with decreasing frequency (ω^4), the spacer spring mode portion of the damping can be subtracted for the purpose of predicting the low frequency thermal noise, resulting in the effective Q's shown in column 5 of Table 3 on page 9. These effective Q's would give a significant reduction in the internal thermal noise in the 40-m interferometer.

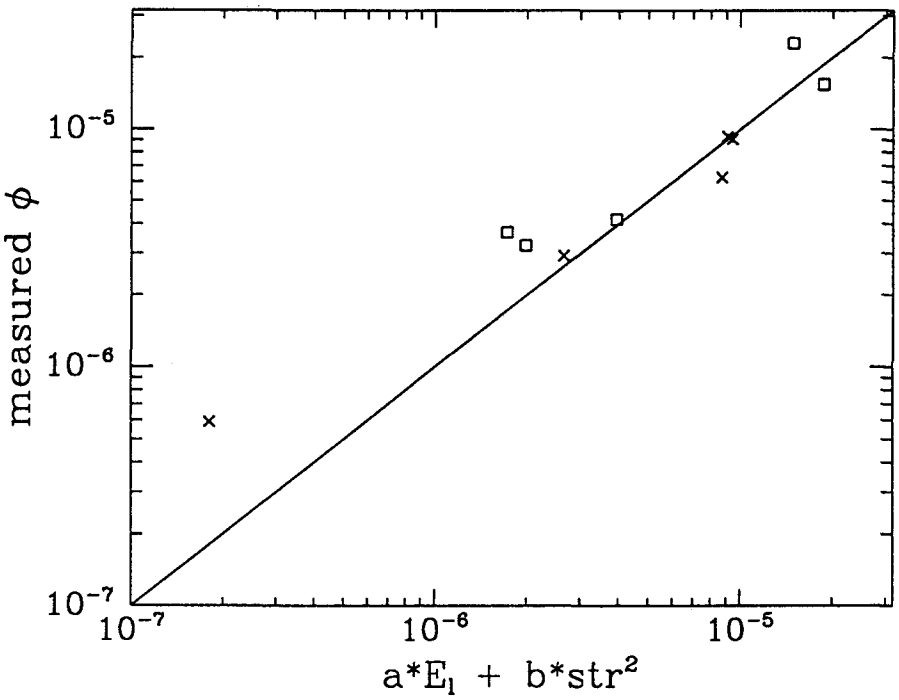

Figure 6: Comparison of measured losses with the model of a combination of strain damping and longitudinal spacer resonance damping. The crosses and the squares indicate measurements taken with the magnets at different locations on the test mass.

3.4 Choice of magnet size

The spacer-magnet assembly had one significant weakness. The assembly had a transverse flexural resonance in the spacer which was at 1.7 kHz, a significantly lower frequency than the longitudinal resonance. This resonance, since it was near the unity gain point of the interferometer locking servo, would make the servo unstable. Calculations based on estimates of how well one could reasonably center the magnet on the spacer and in the coil indicated that for the parameters of this spacer, a gain bump of about a factor of three and maximum additional phase shift of about 90° should be expected. Measured transfer functions were consistent with these estimates. In order to push the transverse resonance to a sufficiently large frequency and maintain the improvement in Q, we were forced to use smaller magnets.[6]

The smaller magnets (on the same size spacers) had a transverse resonant frequency at 5 kHz and a longitudinal resonant frequency at 42 kHz. The measured Q values and the effective low frequency Q values are given in Table 4 on page 14 (this table gives the Q's of the test masses which were installed in the 40-meter interferometer). The effective Q's for this system were better than for the larger magnet system, and it was adopted as the configuration to install in the 40-meter

6.There was some risk in the decision to change the magnet size in that we were far from certain that the interferometer would acquire lock with the smaller magnets. In addition, even if the interferometer did acquire lock, the smaller magnets would require that in order to obtain optimal performance adjustments in the servo would have to be made, thus coupling servo changes with test mass changes and complicating the project.

interferometer.
In addition to test a spacer design with smaller magnets, several alternative spacer designs were investigated to increase the transverse resonant frequency and maintain the larger magnets. These included designs using hollow cylinders, designs with shorter spacers, and designs using three small rods widely spaced on the test mass. Steel and fused silica spacer material were also investigated. None of these alternatives gave as good results as the aluminum spacer with the small magnets.

3.5 Test mass design criteria

Having achieved good results with a trial and error experimental program, the important aspects of the test mass designs can be identified. The most important aspect of the design is the magnets. To achieve good Q results one should carefully consider how to minimize the magnet size and, if possible, consider alternative designs that do without magnets altogether. The smaller the magnet is, the smaller the surface area contact one can have and the smaller the mass on the spacer will be allowing for higher frequency spacer resonances.
Once the magnet size is chosen, one must choose a magnet and spacer geometry. There are two driving design criteria. To maximize the Q, the strain energy coupled to the magnets must be minimized. Long, thin spacers tend to minimize strain energy coupling. There is the additional constraint that the transverse resonant frequency must be large enough to avoid servo problems. Short, thick spacers have large resonant frequencies. With these criteria the relative merits of various spacer aspect ratios could be explored using finite element analysis.
In addition to these basic design criteria, one must also keep in mind quality control. With small surface area contacts, one must worry about the quality of the glue joints. For our spacer size we found that approximately 5% of the joints gave abnormally low Q's. If one considers two glue joints per spacer, four magnets per mass, and four masses per interferometer, there is a high probability of getting a bad glue joint. Each set of glue joints was tested before installation and one was redone. Probably if one makes the surface area smaller the reproducibility of the glue joint may become worse.
Another quality issue is that the long, thin spacer design is fragile. Installation of a test mass requires considerable handling through a glue joint test, a vacuum bake, an optical test, and the physical installation procedure. Our success rate without breaking off a magnet was only 50%. Any new test mass design should make provisions for careful handling throughout these procedures.
Of lesser importance than the magnets are the wire attachments. The data show that by using relatively small fused silica wire attachment points the wires can be made to contribute relatively little additional loss. Probably this loss can be made even smaller with smaller attachment points, but then the difficulties in handling and placing such small pieces must be considered.

4 INSTALLATION IN THE 40-METER INTERFEROMETER

4.1 New internal thermal noise

The new test masses were installed in the 40-meter interferometer. The end masses (shown schematically in Figure 7 on page 13) had the small magnets attached to them with the spacer design.

The vertex masses had no magnets attached to them. The end masses had their wires placed 76 mm apart and the vertex masses had their wires placed 25 mm apart (the difference was due to differences in the existing control blocks of the two types of suspensions). In addition, the vertex masses had a 0.5° wedge and the end masses had a 2° wedge. The difference in wedge angle made the resonant frequencies slightly different.

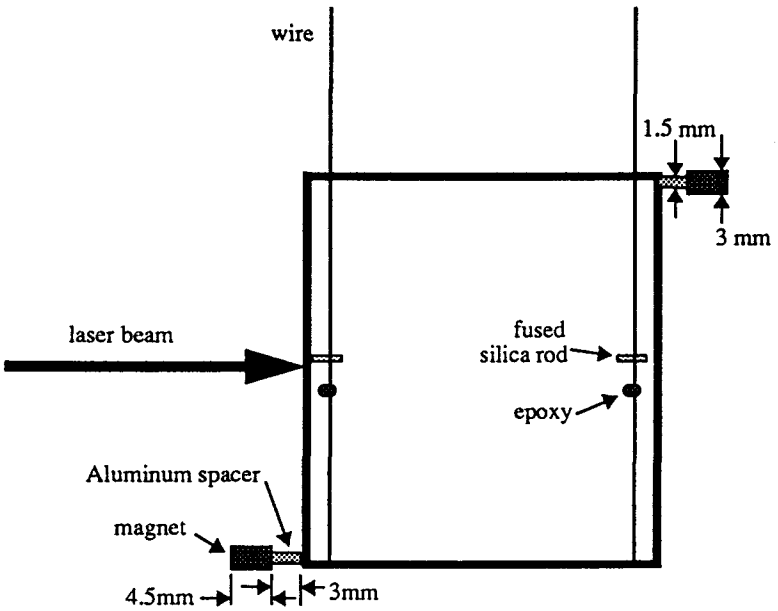

Figure 7: Schematic view of an end test mass as suspended in the 40-m interferometer.

The measured Q's of all of the masses and the effective Q's of the end masses are shown in Table 4 on page 14. The modes are the five modes shown in Figure 3 on page 6. The fifth mode is not listed for the end masses because the large wedge angle caused mixing of that mode with a non-axisymmetric mode which made its identification ambiguous.

These Q's gave a dramatic decrease in the thermal noise. Figure 8 on page 15 shows the noise spectrum for the 40-meter interferometer after the installation of the new test masses and the adjustment of the servo. Also plotted on the figure is the internal vibrational thermal noise prediction of the new masses. To make this estimate, the effective low frequency Q's were used, and the loss function was assumed to be independent of frequency. There is no compelling reason to believe that the loss function should be independent of frequency for the new test masses, it was simply chosen because it explained the data from the old test masses. The assumption that the loss function was independent of frequency is conservative. If the loss function were much larger, excess noise would be observed with the interferometer; however the loss function could be substantially lower without our knowing it.

In addition to considering the 18 modes in Table 4 on page 14, all other modes with acoustic wavelengths greater than the laser spot size were included. The loss function for these modes was assumed to be the average loss function for the modes of each particular mass. Also, the thermal noise due to the longitudinal resonances of the spacers were included. The fact that the spacer was heavily damped with a Q of about 25 compensated for the factor of 5000 mass difference between the magnet and the test mass to make the spacer mode's thermal noise be of the same order of magnitude as the test mass modes' thermal noise.

For comparison the figure also includes the old interferometer noise and thermal noise estimate

Table 4: Q's of new test masses as installed in 40-meter interferometer.

test mass	*resonant frequency (Hz)*	*measured Q (10^3)*	*effective low frequency Q (10^3)*
East End	30371	200	510
	31178	680	>5,000
	35125	43	530
	39369	79	2,500
East Vertex	30196	3,900	
	30751	8,100	
	34776	1,700	
	38967	3,300	
	44035	5,800	
South Vertex	30192	5,900	
	30719	6,100	
	34693	1,700	
	38942	2,200	
	43997	4,600	
South End	30102	190	430
	31104	850	>5,000
	34995	40	460
	39190	60	2,200

(see Figure 1 on page 4), as well as the new shot noise prediction. The shot noise prediction and the improvement in the high frequency portion of the spectrum indicate the improved optical quality of the new mirrors.

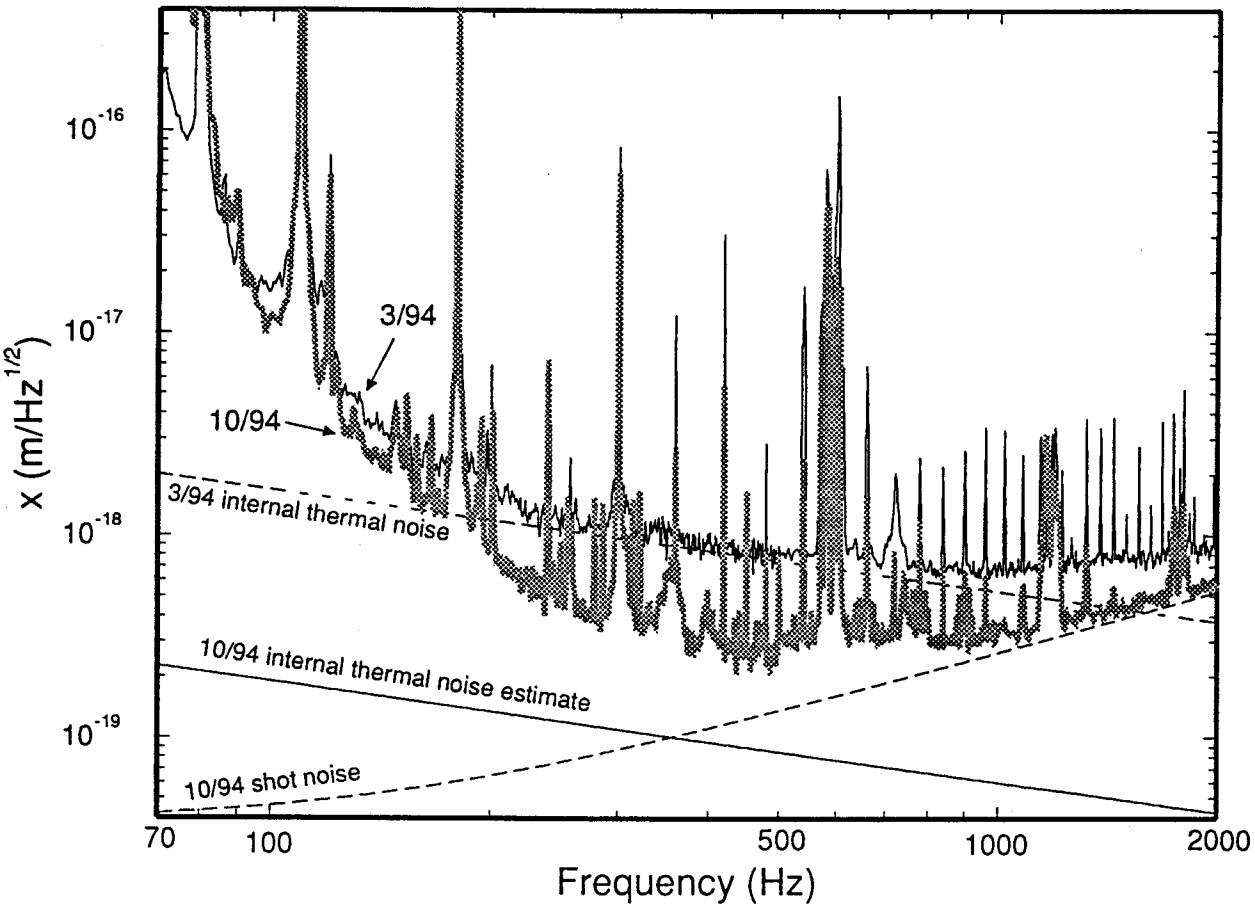

Figure 8: 40-meter interferometer displacement noise in October 1994, along with the 10/94 shot noise and internal vibrational thermal noise estimates. For comparison the March 1994 noise spectrum and internal vibrational thermal noise estimates are also plotted.

4.2 Total thermal noise

In addition to replacing the test masses, the suspension wires were also replaced. The new violin mode Q's are given in Table 5 on page 16. The pendulum mode loss function can be partially predicted from the violin mode Q's.[7] From those loss functions the thermal noise due to the suspensions can be predicted. The violin mode losses do not reflect damping forces that act directly on the test mass. Such a force that is important in the 40-meter interferometer is the eddy current damping of the pendulum due to the magnets attached to the mass and the magnet driving coils.

For the 40-meter interferometer, the force to current ratio was 2.025×10^{-2} newtons/ampere and the output impedance of the coil drivers was 70 ohms for one arm and 220 ohms for the other (the differences are due to historical servo evolution). The noise spectrum along with all three thermal noise sources--internal vibrational thermal noise, suspension thermal noise in the wires,

7. A. Gillespie and F. Raab, Suspension losses in the pendula of laser-interferometer gravitational-wave detectors, *Phys Lett A*, **190** 213 (1994); A. Gillespie and F. Raab, Thermal noise in the test mass suspensions of a laser interferometer gravitational-wave detector prototype, *Phys Lett A*, **178** 357(1993).

and eddy current damping thermal noise in the pendulum--are plotted in Figure 9 on page 17. This plot is the complete thermal noise prediction of the 40-meter interferometer as of October 1994.

Table 5: Violin mode Q's.

test mass	*violin mode resonant frequency (Hz)*	*Q (10^3)*
east end	571.60 578.40 594.25 599.00	80 360 50 140
east vertex	581.10 584.00 595.98 597.68	94 81 117 100
south vertex	585.02 593.98 597.72 598.50	70 190 140 150
south end	578.72 582.42 597.98 605.42	70 88 78 31

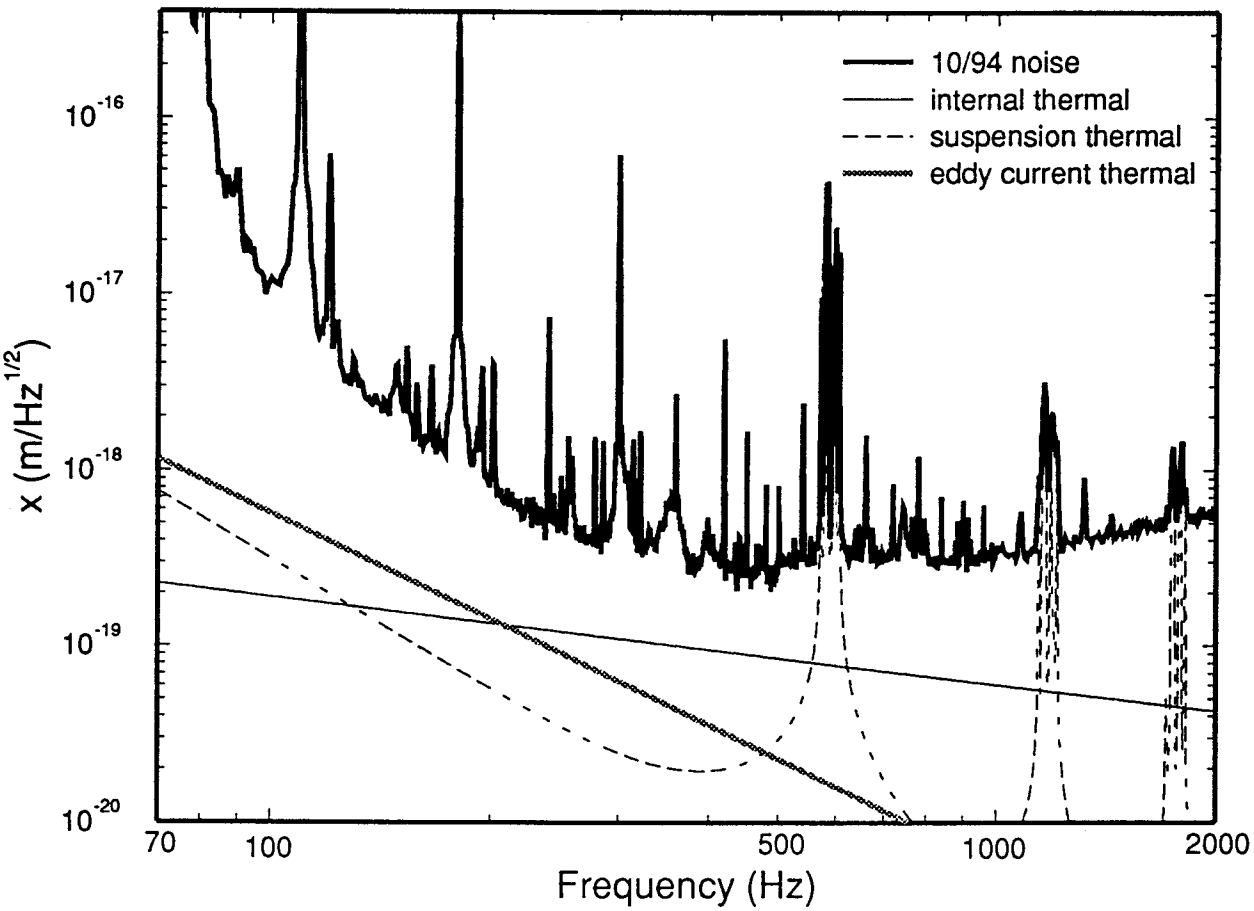

Figure 9: Total thermal noise of 40-meter interferometer as of October 1994.

DISTRIBUTION FOR ATTACHED DOCUMENT
LIGO-T950029-00-R

NAME	RM	NAME	RM	NAME	RM
CIT:					
Abramovici, Alex	352C WB	Barish, Barry	M/C	Blackburn, Kent	
Camp, Jordan	361 WB	Durance, Denise	40M Lab	Jungwirth, Doug	28 BA
Kawamura, Seiji	361 WB	Kuhnert, Andy	359 WB	Lazzarini, Albert	363 WB
Raab, Fred	354 WB	Sanders, Gary	101 EB	Savage, Rick	359 WB
Sievers, Lisa	352 WB	Solomonson, N.		Spero, Robert	352 WB
Vogt, Robbie	102 EB	Yamamoto, Hiro	352 WB		
CIT GRAD STUDENTS:					
Carri, John	356 WB	Lyons, Torrey	356 WB	Mason, James	356 WB
Rakhmanov, Malik	356 WB				
MIT:					
Fritschel, Peter		Gonzalez, Gabriella		Hefetz, Yaron	
Shoemaker, David		Weiss, Rai		Zucker, Mike	

LASER INTERFEROMETER GRAVITATIONAL WAVE OBSERVATORY

- LIGO -

CALIFORNIA INSTITUTE OF TECHNOLOGY
MASSACHUSETTS INSTITUTE OF TECHNOLOGY

technical note	**LIGO-T950029-00 -R**		4/28/95
Document Type	*Doc Number*	*Group-Id*	*Date*

Installation of the New Test Masses

Title

Aaron Gillespie

Author(s)

This is an internal working note
of the LIGO Project

California Institute of Technology
LIGO Project - MS 102-33
Pasadena CA 91125
Phone (818) 395-2966
Fax (818) 304-9834
E-mail: info@ligo.caltech.edu
WWW: http://www.ligo.caltech.edu

file /tmp_mnt/home/manx3/aaron/papers/testmass - printed May 3, 1995

1 ABSTRACT

This paper is a complete summary of recently completed work to install new test masses in the 40-meter inteferometer at Caltech. It is intended to be used primarily within the LIGO project for documentation. Discussed here are the motivations for the work including some history and the thermal noise predictions of the old test masses, a detailed description of the experimental work done in the suspension development apparatus which lead to the present design of the magnet attachments, and the results of the installation of the new test masses. A less detailed report which concentrates only on the results of the installation in the 40-meter interferometer is available in LIGO technical report TR94-7.

2 MOTIVATION

2.1 Background

In late 1991 and early 1992 two improvements were made in the interferometer's performance which increased the priority of the installation of the new test masses. First, new orientation control systems were installed which greatly reduced the noise below 1 kHz,[1] and second, the laser power at the input of the interferometer was increased, reducing the shot noise and thus improving the interferometer performance at higher frequencies. These two improvements left a region in the noise spectrum between 500 Hz and 1.5 kHz where the noise was a slowly varying function of frequency and of unknown origin (see Figure 1 on page 4).

In attempting to explain this region of the noise spectrum, many potential noise sources were ruled out. Any sort of mechanical excitation above thermal noise transmitted through the suspension wires could be ruled out since the violin resonances were at thermally excited levels.[2] Frequency noise and amplitude noise on the light and electronics noise in the readout and coil driver were measured and eliminated as potential noise sources. Noise due to scattered light was a possibility because there was much scattered light in the restricted vacuum system of the 40-meter at that time, but there were no models describing how the scattered light would couple to the interferometer noise at the observed level. In 1993, the Mark II version of the interferometer with its expanded vacuum system became operational. That change made a qualitatively radical change in the scattered light, but the unexplained region of the interferometer noise spectrum remained unchanged, eliminating scattered light as a likely noise source. In addition, the improvements in the seismic isolation of the Mark II reduced the seismic noise, extending the unexplained and slowly varying region of the noise spectrum down to 200 Hz (Figure 1 on page 4).

2.2 Internal thermal noise

One remaining possibility for this noise was thermal noise in the internal vibrations of the test mass. The mechanical quality factors of the old test masses were measured and found to be lower than expected from measurements done before the test masses were installed. The existing test

1. S. Kawamura and M. Zucker, Mirror-orientation noise in a Fabry-Perot interferometer gravitational-wave detector, *Appl Opt.*, **33** 3912 (1994).
2. A. Gillespie and F. Raab, Thermal noise in the test mass suspensions of a laser interferometer gravitational-wave detector prototype, *Phys Lett A*, **178** 357 (1993).

masses were fused silica cylinders 10 cm in diameter and 8.8 cm long. A 25 mm hole was bored through the center and a 38 mm mirror was optically contacted on one face. The faces of the test masses were polished; the sides were not. A summary of the measurements of the Q's of the axisymmetric modes of these test masses are in Table 1 on page 2. The Q measurements were made by sweeping a driving force through the resonance and measuring the FWHM of the frequency response of the interferometer output. For the end masses the driving force was applied by the driving coils near magnets attached to the masses; for the vertex masses the driving force was elctrostatic. These modes were identified as the axisymmetric modes by the following procedure. The approximate resonant frequencies of the axisymmetric modes were found using finite element analysis. The most strongly excited modes near the appropriate frequency were identified as the axisymmetric modes. (Non-axisymmetric modes have nodes at the mirror center where the light sampled the motion and hence are weakly coupled to the interferometer.)

Table 1: Q's of old test masses as installed in 40-meter interferometer.

mirror	*resonant frequency (Hz)*	*Q*
East End	27416 27673 34748	2700 5100 33100
East Vertex	27240 27580	800 2000
South Vertex	27395 27576	30000 1700
South End	27436 27996 34748	54900 14400 41100

The spectral density of the displacement, $S_x(f)$, due to the thermal noise of the internal vibrational modes can be calculated by summing the general thermal noise lineshape over all modes:[3]

$$S_x(f) = \sum_n \frac{4k_B T \varphi_n(\omega)}{\alpha_n m \omega_n^2 \omega}$$

k_B, T, m, and α_n are Boltzman's constant, the temperature, the mass, and the effective mass coefficient of the n^{th} mode; and ω, ω_n, and $\varphi_n(\omega)$ are the angular frequency (corresponding to $2\pi f$), the angular resonant frequency of the n^{th} mode, and the loss function of the n^{th} mode. In order to estimate the off resonance thermal noise from these Q's, several assumptions must be

3. A. Gillespie and F. Raab, Thermally excited vibrations of the mirrors of laser interferometer gravitational-wave detectors, to be published in *Phys Rev D*, (1995).

made. First, the loss function was assumed to be independent of frequency. This assumption enabled the loss function to be defined as

$$\varphi_n(\omega) = \frac{1}{Q_n}$$

This assumption was driven primarily by a desire to get a thermal noise prediction that was close to the measured noise spectrum. Any weak frequency dependence could give the appropriate noise level. Second, the effective mass coefficients must be determined. Since these masses were not solid right circular cylinders, calculation of the coefficients was difficult. We simply assumed effective mass coefficients of 0.5 for all modes. Lastly, one must decide how many modes to consider. In principle, all modes with acoustic wavelengths larger than the laser spot size could contribute to the low frequency thermal noise. In this case, all the modes had different Q's, and determining the Q's of the higher order modes was not possible. We assumed that the noise was dominated by the few lower frequency low Q modes that were measured and did not include the higher order modes.

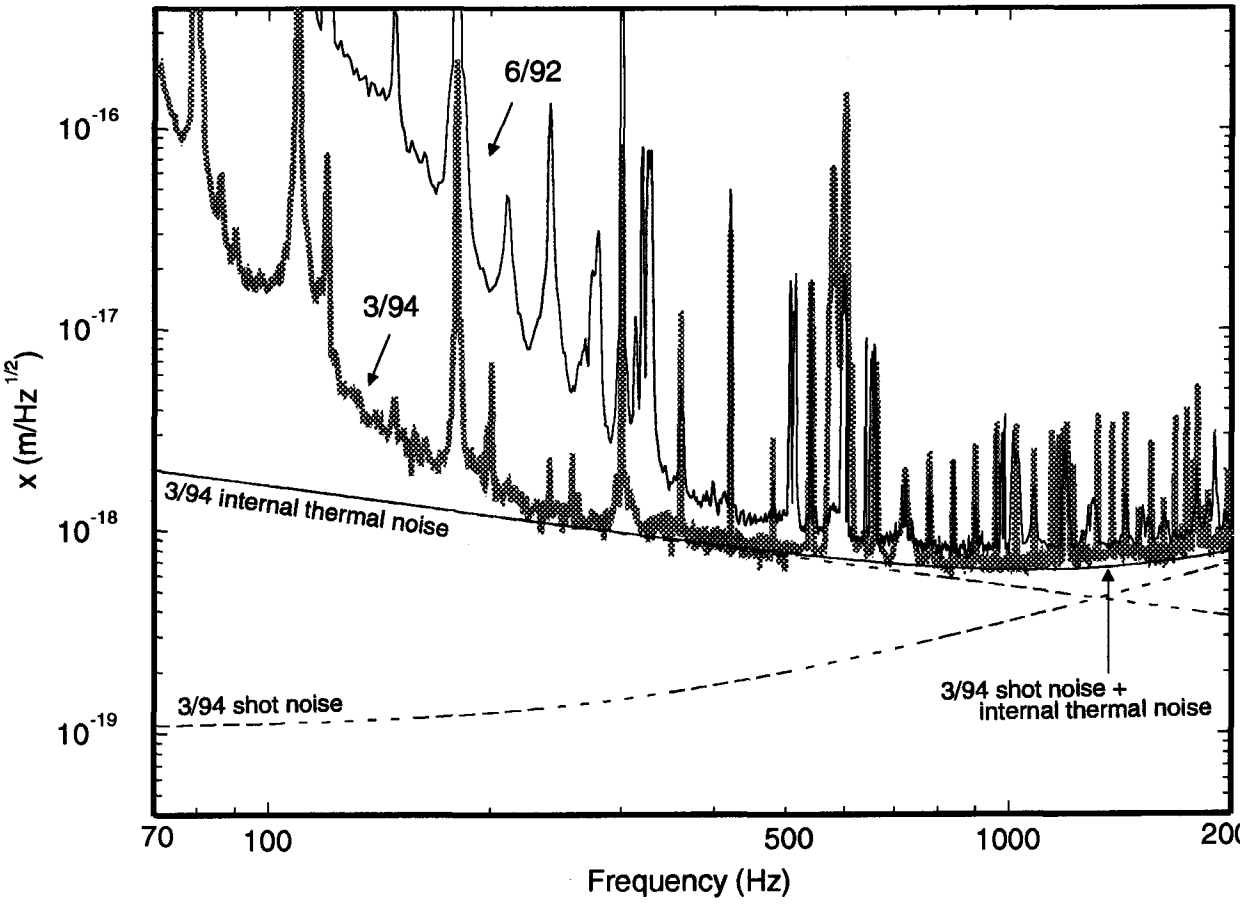

Figure 1: 40-meter interferometer noise spectrum in March 1994. Also shown are the internal vibrational thermal noise estimate and the shot noise.

Given these assumptions, the predicted noise level at 500 Hz was 8×10^{-19} m/$\sqrt{Hz}$, consistent with the observed noise level. The prediction of the internal thermal noise, the predicted shot noise, and the noise spectrum are shown in Figure 1 on page 4. The absolute level of the noise

was adjusted (by 10%), keeping the shape fixed, to give maximum agreement between the noise prediction of internal thermal noise plus shot noise to the observed noise spectrum. Such an adjustment was justified given the uncertainties of the prediction; in fact we were prepared to allow an adjustment of up to a factor of 3. The thermal noise plus shot noise model gave excellent agreement with the noise spectrum above 250 Hz. With this prediction, reduction of internal thermal noise was made a priority after the shakedown of the Mark II interferometer.

3 EXPERIMENTS TO IMPROVE THE Q

3.1 Starting point

An experimental program to improve the Q's of the test mass was begun in early 1992. The old test masses would be replaced with new test masses that had been ordered. The new test mass were 10 cm diameter and 8.8 cm long solid fused silica cylinders. They were polished on all surfaces and had the mirror surface coated directly on one face. The new mirrors had the apparent advantages of their monolithic design (no optical contacts) and their polish on all surfaces. These properties were fixed and their effects were not investigated; they are believed to be improvements. The new mirrors were also higher optical quality.

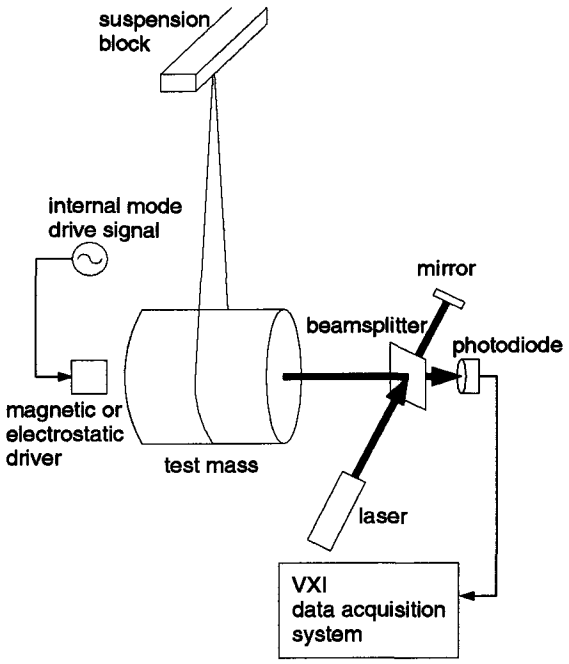

Figure 2: Schematic view of the suspension development apparatus.

The suspension development apparatus, shown schematically in Figure 2 on page 5 was used to evaluate the Q's of various test mass suspension configurations. The Q's were determined by exciting a particular resonance, turning off the excitation, and measuring the decay time of the oscillation. For configurations with magnets, a magnetic driver was used to excite the resonance; for configurations with no magnets, an electrostatic driver[4] was used. For each suspension config-

4. A. Cadez and A. Abramovici, Measuring high mechanical quality factors of bodies made of bare insulating materials, *J Phys E: Sci Instrum,* **21** 453 (1988).

uration, the Q's of the five lowest frequency axisymmetric modes, shown in Figure 3 on page 6, were evaluated.

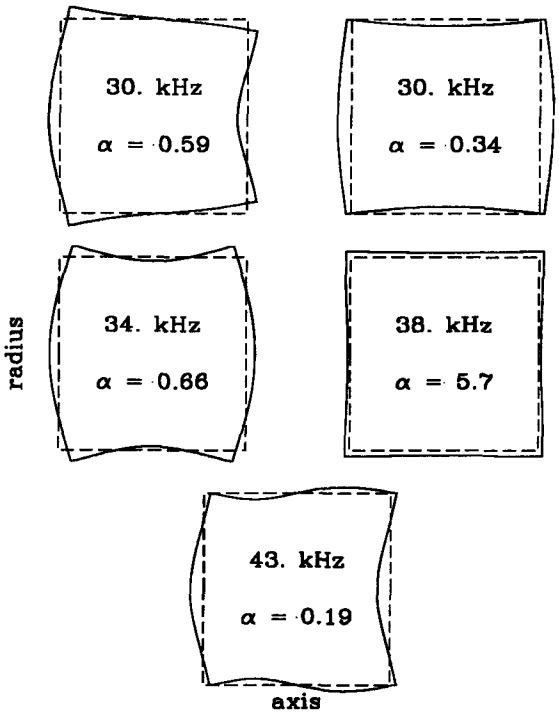

Figure 3: Five lowest frequency axisymmetric modes.

3.2 Initial Measurements

The simplest suspension configuration, and the one in which the least additional loss above the intrinsic loss in the fused silica might be expected, is to suspend the test mass in a single wire loop with no magnets attached. The results of such a set of measurements are given in Table 2 on page 7. The Q's of all modes except the 30.2 kHz mode were above 5×10^6. The 30.2 kHz mode was excessively damped by the suspension wire. That mode is the only one with substantial axial motion at the center where the wire is situated (see the left 30 kHz mode in Figure 3 on page 6). With no well defined attachment point, the wire was free to rub against the side of the test mass as the test mass vibrated in that mode.

In the next two configurations the suspension wires were moved to the positions which they would occupy in the interferometer. Two wire loops were placed 25 mm apart. In one case the test mass simply sat in the wire loops, in another the points at which the wires leave the mass were defined by epoxying small (1 mm diameter by 3 mm long) fused silica rods on the test mass. Results from these two configurations are shown in the second and third columns of Table 2 on page 7. Notice that the Q's in four modes are slightly degraded from the single wire loop configuration, but with the wires position better defined, the 30.2 kHz mode's Q actually improved. The configuration with the fused silica rods was adopted for the vertex masses in the 40-meter interferometer (see Table 5 on page 16).

The test masses used at the ends of the 40-meter interferometer required magnets be attached to

them for control purposes. Column 4 of Table 2 on page 7 shows the Q's when two 6 mm diameter by 6 mm long neodymium-iron-boron magnets were glued near the edges of the mass. The Q's were degraded by three orders of magnitude for some modes and varied by several orders of magnitude among the modes. To test whether this degradation was a property of the magnetic field, the magnets were baked at 200 C for two weeks to reduce their dipole moments to 0.5% of their original values. The data for the demagnetized magnets is shown in column 5 of Table 2 on page 7. The magnetic field strength had no effect on the Q's. In addition, to test for the possibility that the glue was responsible for the additional loss, two different types of glue were used: a cyano-acrylate glue and a vacuum sealant epoxy. There was no difference in the Q's depending on the type of glue. These results indicated that the dominant loss mechanism was due to the magnets themselves and not due to the magnetic field or the glue joints.

Table 2: Test mass Q's: effects of attachments.

mode resonant frequency (kHz)	*simple single loop* $Q\,(10^3)$	*2 wire loops* $Q\,(10^3)$	*with fused silica rods* $Q\,(10^3)$	*with magnets* $Q\,(10^3)$	*demagnetized magnets* $Q\,(10^3)$
30.2	230	3,200	3,600	9.8	8.6
30.7	9,100	7,100	1,800	890	830
34.7	5,700	4,500	3,100	3.3	3.0
39.0	6,900		940		20.
44.0	5,500	8,100	7,300		180.

3.3 Reducing the losses due to the magnets

The magnitude of the losses in the new masses due to the magnets were of the same order as the losses of the old existing masses in the 40-m interferometer (Table 1 on page 3). Therefore in order to make a substantial improvement in the interferometer noise performance, the exact nature of the loss mechanism was investigated. There are three simple ways in which mechanical energy can be coupled into the magnets from the test mass. One is through motion perpendicular to the attachment joint, or axial motion; another is through motion parallel to the connection joint, or radial motion; and the last is through expansion across the connection joint, or strain motion. The amounts of each of these motions at the point of the magnet attachment were computed for each mode, and quantities that were inversely proportional to the energy were constructed. These constructed quantities--(1/axial motion^2), (1/radial motion^2), and (1/strain^2)--would be proportional to the Q if that particular type of energy transfer dominated the losses. The measured Q's were plotted against these constructed quantities to look for proportionalities.

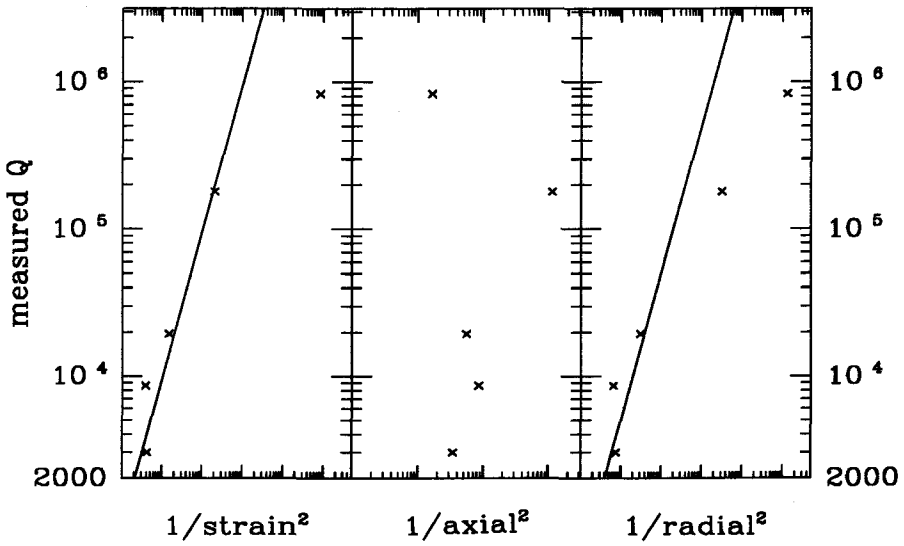

Figure 4: Comparison of measured Q with 3 possible loss mechanisms: couplings of strain energy, axial motion energy, and radial motion energy into the magnets.

Such a plot is shown in Figure 4 on page 8. The demagnetized magnet data were used since those data were most complete.[5] At the factor of three level, four points of the strain damping model and three points of the radial motion damping model lie on a line of direct proportionality. The axial damping motion can be ruled out. For both the strain damping model and the radial damping model, the points that do not fit on the line are the higher Q modes, which have additional damping. There could be some additional damping mechanism that dominates the weakly damped modes but not the strongly damped modes. If the points had fallen on the other side of the proportionality line, or were insufficiently damped in a particular model, then that model could have been ruled out.

Distinguishing between the strain and radial damping models requires additional information which is not on the plot. For the four lowest frequency modes, the face of the test mass undergoes uniform expansion, so that the strain at a particular point is proportional to the radial motion (see Figure 3 on page 6). Only the 43 kHz mode does not have uniform expansion across the face of the mass. This fact is why the radial and strain damping model plots look similar except for at one point. That point is the mode with the Q of 180,000. For the strain damping model the point lies on the direct proportionality line and for the radial damping model it does not. For this reason, the strain damping model was the strongest candidate for the cause of the damping.

Strain energy is coupled between two elements through a surface area. Therefore, the most logical step to minimize the damping would be to minimize the area of contact between the magnet and the test mass. The first step was to verify that this worked, so smaller (3 mm diameter by 5 mm long) magnets were attached to the mass and the Q's were measured. These results are shown in

5. Chronologically, the measurement with the magnets attached was the earliest measurement made. At that time the interferometer was not sensitive enough to measure the Q's of the two higher frequency modes. Since the demagnetized magnet Q's were equivalent to the magnetized magnet Q's for three modes, they were assumed to be equivalent for all modes, and the magnetized magnet measurement was never repeated with the more sensitive interferometer.

column 2 of Table 3 on page 9. The Q's were increased by factors of approximately four for all modes. This improvement was consistent with the hypothesis that the dominant loss mechanism was the coupling of strain into the magnets, but was not sufficient to meet the goal of reducing convincingly the noise in the 40-m interferometer. It was also apparent that magnets which were small enough to meet the goal probably could not be used.

To further reduce the damping, the magnets were not attached directly to the test mass, but rather thin spacers were inserted between the magnets and the masses to attenuate the strain reaching the magnets. Aluminum (for speed and ease of construction) spacers 1.5 mm in diameter and 3 mm long were designed. The Q's were measured with the spacers (and no magnets) attached to the test mass (column 3 of Table 3 on page 9). The results were very promising, so the large magnets were attached to the ends of the spacers. Those Q's are given in column 4 of Table 3 on page 9. The low Q's obtained with the spacers and magnets were initially disappointing and could not be explained with the simple axial, radial, and strain damping models. A full explanation required the consideration of the resonances of the spacer.

Table 3: Test mass Q's: effects of the magnets and spacers.

resonant frequency (kHz)	*with large magnets* $Q\,(10^3)$	*with small magnets* $Q\,(10^3)$	*with Al spacers only* $Q\,(10^3)$	*spacers and big magnets* $Q\,(10^3)$	*effective low frequency* $Q\,(10^3)$
30.2	8.6	44.	1,600	86	190
30.7	830	4,000	3,600	250	4,500
34.7	3.0	9.1	970	53	200
39.0	20.		2,600	350	940
44.0	180	380	1,300	400	1,500

The observed losses could be explained by damping due to a combination of strain transmitted through the aluminum spacer to the magnet and axial motion coupled into the longitudinal spring mode of the aluminum spacer. The energy coupled into the longitudinal spring mode as a function of frequency is

$$E(\omega) \propto \frac{\omega^4}{\left(\omega_0^2 - \omega^2\right)^2 + \omega^4 \varphi_{spacer}^2(\omega)} x_{axial}^2$$

(the damping is proportional to the energy coupled into the spacer). A plot of such a function is given in Figure 5 on page 10. Well below the resonant frequency, the spacer acts as a rigid body. It is not compressed and no energy is coupled into it. Well above the resonant frequency the spacer is compressed and stretched by the amount of the axial motion and the energy coupling becomes independent of frequency. Near the resonant frequency, the spacer resonance is excited and the damping is enhanced.

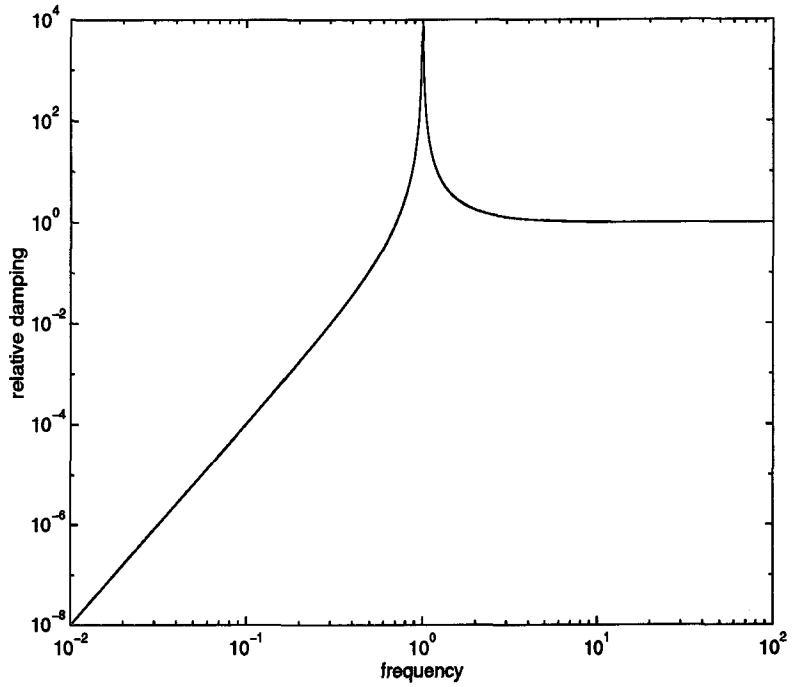

Figure 5: Damping function of test mass due longitudinal spacer mode. On this plot $\omega_0 = 1.$ **and** $\varphi_{spacer}(\omega) = 0.01.$

The measured losses are compared to the model of strain damping plus longitudinal spring mode damping in Figure 6 on page 11. The spacer resonant frequency was about 25 kHz. The ten points came from two sets of measurements on the five modes. One set of measurements was done with the magnets and spacers attached 13 mm from the edge of the mass and the other was done with the magnets at the edge of the test mass. These two sets gave two different sets of samplings of the strain and axial motion of the test mass and gave the additional number of points necessary to do a multi-parameter fit to the damping model. All of the points agree with the model except a few high Q points which show excess damping.

Since the frequencies of interest for the 40-m interferometer and LIGO (100 Hz-1kHz) are well below the spacer resonant frequency and since the spacer damping falls off quickly with decreasing frequency (ω^4), the spacer spring mode portion of the damping can be subtracted for the purpose of predicting the low frequency thermal noise, resulting in the effective Q's shown in column 5 of Table 3 on page 9. These effective Q's would give a significant reduction in the internal thermal noise in the 40-m interferometer.

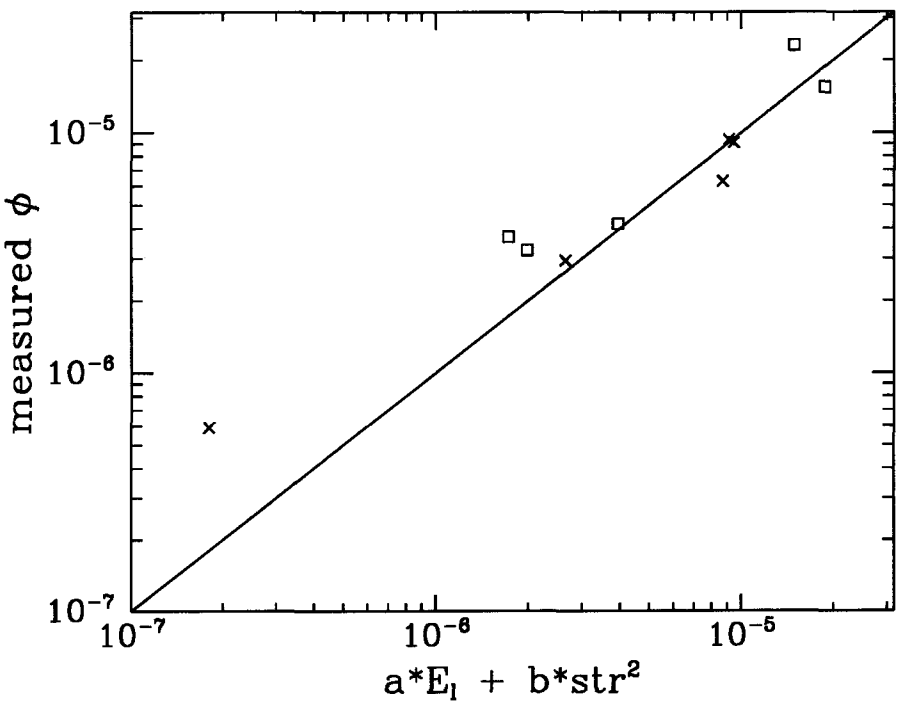

Figure 6: Comparison of measured losses with the model of a combination of strain damping and longitudinal spacer resonance damping. The crosses and the squares indicate measurements taken with the magnets at different locations on the test mass.

3.4 Choice of magnet size

The spacer-magnet assembly had one significant weakness. The assembly had a transverse flexural resonance in the spacer which was at 1.7 kHz, a significantly lower frequency than the longitudinal resonance. This resonance, since it was near the unity gain point of the interferometer locking servo, would make the servo unstable. Calculations based on estimates of how well one could reasonably center the magnet on the spacer and in the coil indicated that for the parameters of this spacer, a gain bump of about a factor of three and maximum additional phase shift of about 90° should be expected. Measured transfer functions were consistent with these estimates. In order to push the transverse resonance to a sufficiently large frequency and maintain the improvement in Q, we were forced to use smaller magnets.[6]

The smaller magnets (on the same size spacers) had a transverse resonant frequency at 5 kHz and a longitudinal resonant frequency at 42 kHz. The measured Q values and the effective low frequency Q values are given in Table 4 on page 14 (this table gives the Q's of the test masses which were installed in the 40-meter interferometer). The effective Q's for this system were better than for the larger magnet system, and it was adopted as the configuration to install in the 40-meter

6.There was some risk in the decision to change the magnet size in that we were far from certain that the interferometer would acquire lock with the smaller magnets. In addition, even if the interferometer did acquire lock, the smaller magnets would require that in order to obtain optimal performance adjustments in the servo would have to be made, thus coupling servo changes with test mass changes and complicating the project.

interferometer.
In addition to test a spacer design with smaller magnets, several alternative spacer designs were investigated to increase the transverse resonant frequency and maintain the larger magnets. These included designs using hollow cylinders, designs with shorter spacers, and designs using three small rods widely spaced on the test mass. Steel and fused silica spacer material were also investigated. None of these alternatives gave as good results as the aluminum spacer with the small magnets.

3.5 Test mass design criteria

Having achieved good results with a trial and error experimental program, the important aspects of the test mass designs can be identified. The most important aspect of the design is the magnets. To achieve good Q results one should carefully consider how to minimize the magnet size and, if possible, consider alternative designs that do without magnets altogether. The smaller the magnet is, the smaller the surface area contact one can have and the smaller the mass on the spacer will be allowing for higher frequency spacer resonances.
Once the magnet size is chosen, one must choose a magnet and spacer geometry. There are two driving design criteria. To maximize the Q, the strain energy coupled to the magnets must be minimized. Long, thin spacers tend to minimize strain energy coupling. There is the additional constraint that the transverse resonant frequency must be large enough to avoid servo problems. Short, thick spacers have large resonant frequencies. With these criteria the relative merits of various spacer aspect ratios could be explored using finite element analysis.
In addition to these basic design criteria, one must also keep in mind quality control. With small surface area contacts, one must worry about the quality of the glue joints. For our spacer size we found that approximately 5% of the joints gave abnormally low Q's. If one considers two glue joints per spacer, four magnets per mass, and four masses per interferometer, there is a high probability of getting a bad glue joint. Each set of glue joints was tested before installation and one was redone. Probably if one makes the surface area smaller the reproducibility of the glue joint may become worse.
Another quality issue is that the long, thin spacer design is fragile. Installation of a test mass requires considerable handling through a glue joint test, a vacuum bake, an optical test, and the physical installation procedure. Our success rate without breaking off a magnet was only 50%. Any new test mass design should make provisions for careful handling throughout these procedures.
Of lesser importance than the magnets are the wire attachments. The data show that by using relatively small fused silica wire attachment points the wires can be made to contribute relatively little additional loss. Probably this loss can be made even smaller with smaller attachment points, but then the difficulties in handling and placing such small pieces must be considered.

4 INSTALLATION IN THE 40-METER INTERFEROMETER

4.1 New internal thermal noise

The new test masses were installed in the 40-meter interferometer. The end masses (shown schematically in Figure 7 on page 13) had the small magnets attached to them with the spacer design.

The vertex masses had no magnets attached to them. The end masses had their wires placed 76 mm apart and the vertex masses had their wires placed 25 mm apart (the difference was due to differences in the existing control blocks of the two types of suspensions). In addition, the vertex masses had a 0.5° wedge and the end masses had a 2° wedge. The difference in wedge angle made the resonant frequencies slightly different.

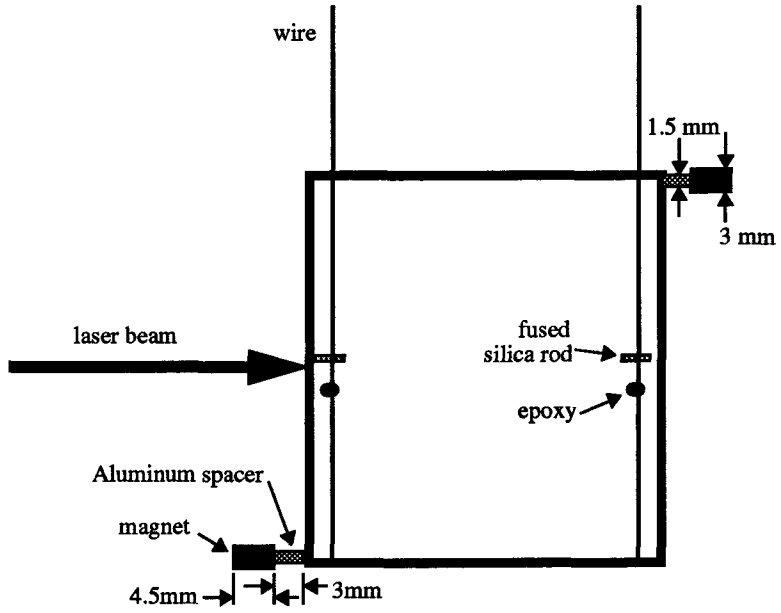

Figure 7: Schematic view of an end test mass as suspended in the 40-m interferometer.

The measured Q's of all of the masses and the effective Q's of the end masses are shown in Table 4 on page 14. The modes are the five modes shown in Figure 3 on page 6. The fifth mode is not listed for the end masses because the large wedge angle caused mixing of that mode with a non-axisymmetric mode which made its identification ambiguous.

These Q's gave a dramatic decrease in the thermal noise. Figure 8 on page 15 shows the noise spectrum for the 40-meter interferometer after the installation of the new test masses and the adjustment of the servo. Also plotted on the figure is the internal vibrational thermal noise prediction of the new masses. To make this estimate, the effective low frequency Q's were used, and the loss function was assumed to be independent of frequency. There is no compelling reason to believe that the loss function should be independent of frequency for the new test masses, it was simply chosen because it explained the data from the old test masses. The assumption that the loss function was independent of frequency is conservative. If the loss function were much larger, excess noise would be observed with the interferometer; however the loss function could be substantially lower without our knowing it.

In addition to considering the 18 modes in Table 4 on page 14, all other modes with acoustic wavelengths greater than the laser spot size were included. The loss function for these modes was assumed to be the average loss function for the modes of each particular mass. Also, the thermal noise due to the longitudinal resonances of the spacers were included. The fact that the spacer was heavily damped with a Q of about 25 compensated for the factor of 5000 mass difference between the magnet and the test mass to make the spacer mode's thermal noise be of the same order of magnitude as the test mass modes' thermal noise.

For comparison the figure also includes the old interferometer noise and thermal noise estimate

Table 4: Q's of new test masses as installed in 40-meter interferometer.

test mass	*resonant frequency (Hz)*	*measured Q (10^3)*	*effective low frequency Q (10^3)*
East End	30371	200	510
	31178	680	>5,000
	35125	43	530
	39369	79	2,500
East Vertex	30196	3,900	
	30751	8,100	
	34776	1,700	
	38967	3,300	
	44035	5,800	
South Vertex	30192	5,900	
	30719	6,100	
	34693	1,700	
	38942	2,200	
	43997	4,600	
South End	30102	190	430
	31104	850	>5,000
	34995	40	460
	39190	60	2,200

(see Figure 1 on page 4), as well as the new shot noise prediction. The shot noise prediction and the improvement in the high frequency portion of the spectrum indicate the improved optical quality of the new mirrors.

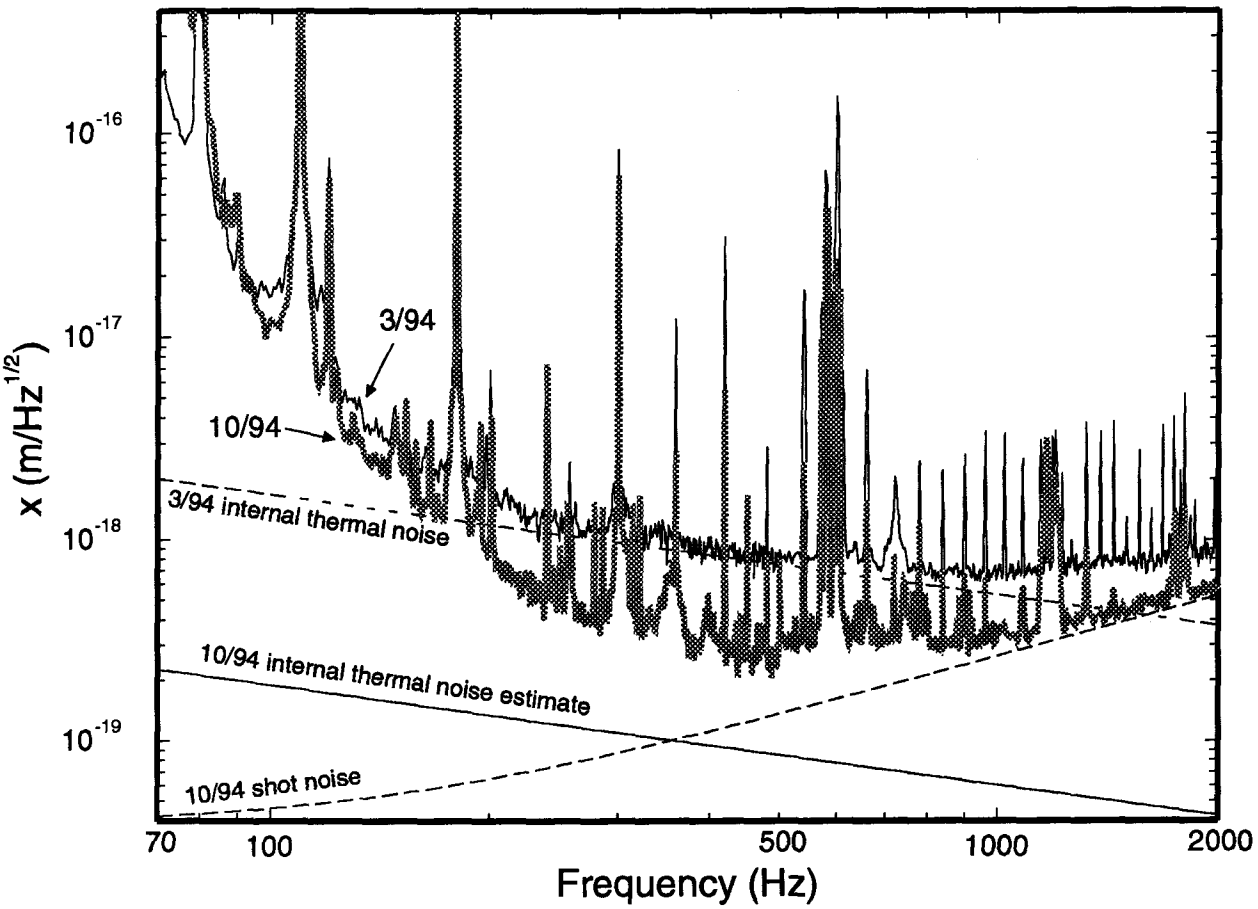

Figure 8: 40-meter interferometer displacement noise in October 1994, along with the 10/94 shot noise and internal vibrational thermal noise estimates. For comparison the March 1994 noise spectrum and internal vibrational thermal noise estimates are also plotted.

4.2 Total thermal noise

In addition to replacing the test masses, the suspension wires were also replaced. The new violin mode Q's are given in Table 5 on page 16. The pendulum mode loss function can be partially predicted from the violin mode Q's.[7] From those loss functions the thermal noise due to the suspensions can be predicted. The violin mode losses do not reflect damping forces that act directly on the test mass. Such a force that is important in the 40-meter interferometer is the eddy current damping of the pendulum due to the magnets attached to the mass and the magnet driving coils.

For the 40-meter interferometer, the force to current ratio was 2.025×10^{-2} newtons/ampere and the output impedance of the coil drivers was 70 ohms for one arm and 220 ohms for the other (the differences are due to historical servo evolution). The noise spectrum along with all three thermal noise sources--internal vibrational thermal noise, suspension thermal noise in the wires,

7. A. Gillespie and F. Raab, Suspension losses in the pendula of laser-interferometer gravitational-wave detectors, *Phys Lett A*, **190** 213 (1994); A. Gillespie and F. Raab, Thermal noise in the test mass suspensions of a laser interferometer gravitational-wave detector prototype, *Phys Lett A*, **178** 357(1993).

and eddy current damping thermal noise in the pendulum--are plotted in Figure 9 on page 17. This plot is the complete thermal noise prediction of the 40-meter interferometer as of October 1994.

Table 5: Violin mode Q's.

test mass	*violin mode resonant frequency (Hz)*	*Q (10^3)*
east end	571.60 578.40 594.25 599.00	80 360 50 140
east vertex	581.10 584.00 595.98 597.68	94 81 117 100
south vertex	585.02 593.98 597.72 598.50	70 190 140 150
south end	578.72 582.42 597.98 605.42	70 88 78 31

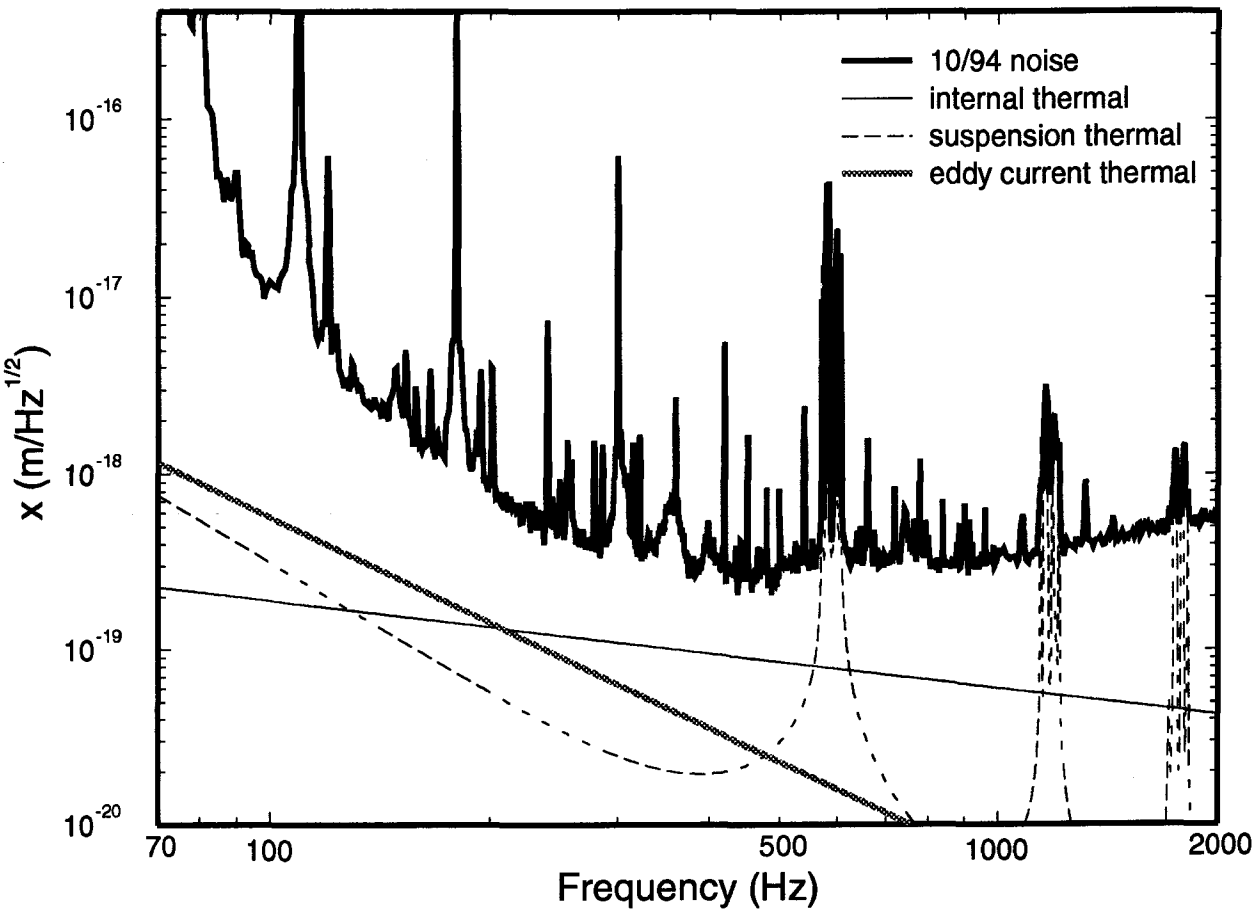

Figure 9: Total thermal noise of 40-meter interferometer as of October 1994.